

1 Mesoscopic surface roughness of ice crystals pervasive across
2 a wide range of ice crystal conditions

3 **N.B Magee¹, A. Miller¹, M. Amaral¹, and A. Cumiskey¹**

4 [1]{The College of New Jersey, Ewing, NJ}

5 Correspondence to: N.B. Magee (magee@tcnj.com)

6

7 **Abstract**

8 Here we show high-magnification images of hexagonal ice crystals acquired by
9 Environmental Scanning Electron Microscopy (ESEM). Most ice crystals were grown and
10 sublimated in the water vapor environment of an FEI-Quanta-200 ESEM, but crystals grown
11 in a laboratory diffusion chamber were also transferred intact and imaged via ESEM. All of
12 these images display prominent mesoscopic topography including linear striations, ridges,
13 islands, steps, peaks, pits, and crevasses; the roughness is not observed to be confined to
14 prism facets. The observations represent the most highly magnified images of ice surfaces yet
15 reported and expand the range of conditions where the rough surface features are known to be
16 conspicuous. Microscale surface topography is seen to be ubiquitously present at temperatures
17 ranging from -10°C to -40°C , at super-saturated and sub-saturated conditions, on all crystal
18 facets, and irrespective of substrate. Despite the constant presence of surface roughness, the
19 patterns of roughness are observed to be dramatically different between growing and
20 sublimating crystals, and transferred crystals also display qualitatively different patterns of
21 roughness. Crystals are also demonstrated to sometimes exhibit inhibited growth in
22 moderately supersaturated conditions following exposure to near-equilibrium conditions, a
23 phenomena interpreted as evidence of 2-D nucleation. New knowledge of the characteristics
24 of these features could affect the fundamental understanding of ice surfaces and their physical
25 parameterization in the context of satellite retrievals and cloud modeling. Links to
26 supplemental videos of ice growth and sublimation are provided.

27

28 **1 Introduction**

29 It has been broadly recognized (IPCC 2007; Bony et al. 2006) that cloud-climate feedbacks
30 are the most weakly constrained radiative forcings for general circulation models of a

1 changing future climate. Among the variety of cloud feedbacks that have been identified and
2 parameterized, cirrus clouds are notable for being especially uncertain — even the sign of the
3 likely feedback effect is subject to debate (Mitchell et al. 2008; Burkhardt 2011). Baran
4 (2012) presents a compelling case that the complex radiative scattering properties of
5 heteromorphous ice crystals must be accounted for to reach a physically consistent
6 parameterization of ice clouds in climate models. In addition to cloud-climate feedbacks, it is
7 expected that prominent mesoscopic topography (defined here as variation scale between 100
8 nm and 5 μ m) would affect active research questions in stratospheric ozone chemistry
9 (McNeill et al. 2007) and thunderstorm electrification (Dash et al. 2001). Despite recognition
10 that the microscale structures of ice are critically important to consider, very few images of
11 ice are available at this resolution.

12 While many experimental research efforts have characterized the effects of temperature,
13 supersaturation, and pressure on particle-scale ice crystal growth rates and morphology under
14 conditions relevant to atmospheric processes (Lamb and Hobbs 1971; Kuroda and Lacmann,
15 1982; Bailey and Hallett 2004; Nelson and Knight 1998; Magee et al. 2006), to date the limits
16 of light microscopy have prevented a thorough analysis of the surface details of ice crystals
17 beyond the microscale. Several studies have employed interference techniques or ellipsometry
18 to suggest the presence of surface structure and disorder of ice (Bryant et al. 1960; Furukawa
19 et al. 1987; Sazaki et al. 2010), but no highly-resolved images of mesoscopic surface structure
20 have been available. Early SEM studies examined formvar replicas of ice crystals, and in
21 some instances were successful in revealing crystal structures beyond the resolution of light
22 microscopy (Shaefer 1941; Truxby 1955; Kuroiwa 1969, Goodman et al. 1989). The use of
23 chemical etchants also revealed new information on the nature of lattice defects in ice and
24 provide tantalizing images that are reminiscent of the some of the mesoscopic structures seen
25 in the present work (Truxby 1955; Kuroiwa 1969). Despite the availability of sub-micron
26 details that can be preserved by proper application of formvar replication, several authors
27 have pointed out that the effects of the solvents on the surface are hard to define (e.g.
28 Takahashi 1988). The first scanning electron micrographs of non-replicated ice were made
29 from platinum sputter-coated natural snowflakes by Wergin et al. (1995); their striking
30 images show a variety of complex structures, but due to warm collection conditions and the
31 sputtering processes, they are ambiguous with respect to presence of mesoscopic surface
32 structure (Wergin et al. 1995). Recently, Neshyba et al. (2013), Ulanowski et al. (2014),
33 Petersen et al. (2011), Pfalzgraff et al. (2010), Kuhs et al. (2010), and Zimmerman et al.

1 (2007) have used uncoated, in-situ growth of ice crystals in ESEM or variable-pressure SEM
2 to identify surface roughness in the form of ridges or “trans-prismatic” strands. Through
3 images resolved at up to 10,000x magnification (compared with previous maximum
4 magnifications of ~1000x), our observations underscore this newly emerging view of the ice
5 surface, demonstrating that mesoscopic surface roughness is a non-uniform condition present
6 on a wide array of ice crystals, and is not confined to a narrow range of macroscopic
7 morphology, substrate, temperature, humidity, or growth rates.

8 Over fifty years have passed since the first account of a relationship between surface
9 roughness and specular reflectivity (Bennett and Porteus, 1961). A growing recognition is
10 now emerging that divergence away from the classical smooth-facet assumption for ice will
11 affect the way that light is scattered. A broad suite of recent measurements and models
12 describe the potential effect of surface roughness and complex micro-scale geometry in
13 smoothing the peaks of the ice-scattering phase function (Baran 2012; Baum et al. 2010;
14 Baum et al. 2011; Cotton et al. 2010; Heymsfield et al. 2006; Ulanowski et al. 2006;
15 Ulanowski et al. 2010; Ulanowski et al. 2012; Um and McFarquhar, 2011).

16 Despite acknowledged uncertainty regarding the details of real roughened ice surfaces, a
17 variety of recent studies have concluded that cirrus radiative measurements and models come
18 into better agreement when attempting to account for complicated shapes and rough ice
19 surfaces. For example, Kahnert et al. (2008) estimated that the effect of varying
20 parameterizations of ice surface microphysics can affect the modeled radiative influence of
21 cirrus by a factor of two. Baum et al. (2011) recently determined that assumption of a
22 roughened ice surface results in better fits to ice particle data retrievals from the CALIOP
23 lidar instrument on board the NASA-CALIPSO A-train satellite. Polarized ice-cloud
24 reflectances have also been shown to have high sensitivity to ice particle geometry and texture
25 (Chepfer et al. 2001; Baran and Labonnote 2006). Polarized ice-cloud reflectances measured
26 by PARASOL have been found to agree best with a mixed-habit model of severely-roughened
27 ice particles (Cole et al. 2013) and retrievals indicate the greatest average roughness in ice
28 clouds associated with tropical deep convection (Cole et al. 2014). Mauno et al. also point
29 out discrepancies between measured and modeled cirrus-modulated shortwave radiative
30 fluxes that would be improved by assumption of surface roughness on ice crystals (Mauno,
31 2011). In addition to passive satellite measurements of cirrus ice microphysics, it is also likely
32 that ice scattering functions assumed in radar and lidar imaging of cirrus and mixed-phase
33 cloud properties would be affected (Sun et al. 2011). Because satellite observations, aircraft

1 measurements, and modeling of cirrus and mixed-phase clouds have often been at odds
2 (Baran 2012; Garrett and Gerber 2003; Gierens et al. 2003; Kramer et al. 2009; Harrington et
3 al. 2009; Jensen et al. 2009; McFarquhar et al. 2007; Peter et al. 2006; Connolly et al. 2007),
4 potential artifacts of surface roughness on both satellite retrievals and modeling of ice
5 microphysics must be carefully evaluated.

6 **2 Methods**

7 We employed an FEI Quanta-200 FEG environmental scanning electron microscope (ESEM)
8 to observe ice crystals at temperatures from -10°C to -45°C and through a wide range of
9 under-saturated, equilibrium, and super-saturated vapor pressures. Most experiments
10 examined in-situ nucleation, growth, and sublimation of ice crystals in the pure water vapor
11 environment of the ESEM. Several experiments also included imaging of ice crystals grown
12 in an external diffusion chamber and then transferred into the ESEM.

13 **2.1 In-situ growth and sublimation**

14 In-situ growth and sublimation experiments were conducted on the ESEM stage, with the ice
15 nucleating on a substrate mounted to a Peltier cooling block. An aluminum stub fitted to the
16 Peltier block was machined to expose a 1 mm diameter surface to the chamber environment
17 such that the entire surface could be contained in the ESEM field of view at low
18 magnification. An insulating vinyl mask was used to ensure that ice growth was limited to the
19 intended cold surface. Growth and sublimation experiments were conducted on bare
20 aluminum as well as on a variety of thin substrates that were attached to the aluminum by
21 thermally conductive epoxy. Substrates that were tested included stainless steel, aluminum,
22 and copper, as well as mineral substrates including Covellite, Muscovite, Bismuth, Magnesite,
23 Galena, and Quartz.

24 Once the substrate was mounted onto the Peltier stage, the ambient air in the ESEM chamber
25 was evacuated and back-filled with water vapor, after which the ice growth experiments were
26 initiated. After cooling to a temperature at or above -45°C , ice nucleation, growth, and
27 sublimation was controlled through direct adjustment of the water vapor pressure or surface
28 temperature. Vapor pressure was controlled at 0.5 Pa increments between 0 and 500 Pa via
29 automatic differential pumping. Vapor measurements were made to 0.1 Pa resolution. In a
30 typical experiment, vapor pressure was first adjusted to the equilibrium frost point and
31 subsequently increased in small increments until ice crystal nucleation was observed. A

1 magnification of 100x was employed until ice crystal growth became visible, after which
2 variable resolutions (as high as about 10,000x) were used in to capture detailed images and
3 movies of the growing ice crystals. Maximum image acquisition size for the FEI Quanta200 is
4 4096 x 3775 pixels (~15.5 MP). At 2500x magnification, this results in a single pixel with
5 dimension 25.4 nm x 25.4 nm. At 2500x magnification, we observed that typical imaging
6 conditions resulted in linear features that could be resolved at limits of 2-3 pixels (50-75 nm).
7 With increasing magnification, signal-to-noise reduction partially (but not completely) offset
8 resolution gains, such that we estimate a resolution limit of approximately 25 nm for these
9 methods.

10 In a typical experiment, the differential pumping and thermoelectric cooling of the substrate
11 required approximately 10 minutes to reach equilibrium values of vapor pressure near 65 Pa
12 and -25°C. Temperature of the Peltier block is automatically reported through the FEI
13 instrument software to 0.1°C resolution and the water vapor pressure is reported to 0.1 Pa
14 resolution. Based upon drop freezing measurements, and trials of substrate-free growth, we
15 are confident that vapor pressure values were precisely and accurately controlled and
16 reported; however, we determined that the surface temperature of the substrate was typically
17 several degrees warmer (+0.5 to +6.5 °C) than the temperature indicated for the Peltier base.
18 This offset was determined by observing the (equilibrium) vapor pressure at which ice neither
19 grew nor sublimated and inferring surface temperature from the Murphy and Koop vapor
20 pressure formulation (2005); we observed this thermal offset to vary based on the
21 temperature, the thickness of the substrate, and its thermal conductivity. Additional detail for
22 the calibration of temperature offset and calculated saturation ratio is provided in Appendix
23 A. Following the approach to equilibrium, vapor pressure was raised in 0.5 Pa increments
24 until nucleation of one or several ice crystals occurred. It was frequently challenging to
25 nucleate a single crystal, even with incremental increases in vapor pressure. Once a crystal of
26 interest was developed, it was examined and photographed at a variety of magnifications,
27 ranging from 100x to 10000x and at a variety of vapor densities, including super- and sub-
28 saturated conditions, and through multiple cycles of growth and sublimation.

29 **2.2 Transported Crystals**

30 In order to image crystals grown in the presence of background air pressure and to minimize
31 the role of the growth substrate, we also developed a new technique to grow, capture, and
32 transfer ice crystals from a controlled diffusion chamber into the ESEM. Ice crystals were

1 grown in a diffusion chamber contained within a large-volume, ultra-low temperature freezer.
2 The full freezer volume is held at -55°C and all walls are coated with ice to achieve a
3 saturated environment. The diffusion chamber generates a small region of supersaturation
4 along a thin vertical fiber between two parallel, horizontal ice plates, with the ice surface
5 temperatures maintained by thermoelectric modules. Ice crystals were grown at ambient lab
6 pressure ($\sim 1000\text{ hPa}$), and at low supersaturation ($<110\% \text{ RH}_i$), with temperature near -50°C ,
7 usually with many crystals in close proximity along the fiber. Within the saturated freezer,
8 several dozen of these ice crystals were then captured in a pre-chilled small-volume ($\sim 1\text{ cm}^3$)
9 containment cell. The transfer and sealing process from diffusion chamber to cryo-cell
10 requires just a few seconds, and intentionally avoids any exposure to ambient room air. The
11 base of the containment cell was formed from an aluminum stub to allow direct transfer into
12 the ESEM cooling stage. Upon capture, the cell was sealed closed and transferred to a
13 specially-designed cryogenic dewar (filled with liquid nitrogen or crushed dry ice) for
14 transport to the ESEM. The cell was then removed from the dewar and quickly placed onto
15 the pre-chilled cooling stage of the ESEM. Throughout the capture and transfer process, the
16 primary objective was to allow ESEM imaging of the ice surfaces as they had been growing
17 in the diffusion chamber and without additional sublimation or growth. To prevent unintended
18 sublimation, the small-volume containment cell was filled with many crystals and quickly
19 sealed so that equilibrium vapor pressures would preserve the crystal surfaces. The
20 containment cell was also enveloped by materials with significant heat capacity and the cryo-
21 dewar designed and handled to maintain near isothermal conditions. Once the sealed
22 containment cell was transferred to the ESEM cooling stage, the microscope chamber was
23 evacuated and adjusted to equilibrium vapor pressures matching the cold stage and
24 containment cell temperature. After reaching equilibrium vapor pressure in the ESEM
25 chamber, the containment cell was then opened using electronically driven stage movement to
26 mechanically pull off the top seal. Following unsealing of the containment cell, ESEM
27 imaging could proceed as in the in-situ growth and sublimation experiments.

28

29 **3 Results and discussion**

30 The overriding impression of our experiments suggests that surface structures on the 0.1 to 10
31 micron scale are a ubiquitous feature of ice crystal facets. The morphology of many of these
32 structures agree with observations recently reported by Neshyba et al. (2013), Ulanowski et

1 al. (2014), Pfalzgraff et al. (2010), Petersen et al. (2011), and Zimmerman et al. (2007). Our
2 observations provide new evidence of roughening on basal crystal facets, as well as images
3 and videos at high magnifications (1000x -10000x) that reveal smaller scale roughening that
4 is not readily apparent at magnification below 1000x. Our observations also show strongly
5 different morphology between textures of growing surfaces as compared to sublimating
6 surfaces. The results also include images of ice crystals grown in air-vapor mixtures and then
7 transferred into the ESEM. These images do show mesoscopic surface roughness, but suggest
8 that the presence of air or different modes of internal heat transfer may significantly affect the
9 character of surface texture development.

10 **3.1 Growing Crystals**

11 As described in section 2.1, ice crystals were nucleated and grown on an ESEM cold stage at
12 a variety of temperatures and pressures. Crystals typically nucleated at just a few percent
13 above equilibrium vapor pressures and continued to grow steadily in proportion to the
14 magnitude of ice supersaturation. At high supersaturations $>150\% RH_i$, nucleation and
15 growth proceeded so quickly that it was difficult to isolate and follow the progression of a
16 single crystal, as the entire stage would be overtaken by intersecting crystals within a few
17 seconds. Therefore, most growth experiments occurred at modest supersaturation, usually
18 $105\text{-}125\% RH_i$. While we did observe clear surface morphology differences between growing
19 and sublimating crystals, we did not detect a systematic dependence on the degree of
20 supersaturation, the rate of growth, nor the composition of the underlying substrate.

21 **3.1.1 Roughness morphologies and scales**

22 In our ESEM growth experiments, we observed mesoscopic linear striations on prism faces
23 (Figure 1e-g) similar to those described by Neshyba et al. (2013) and Pfalzgraff et al (2010)
24 as well as a variety of other mesoscopic roughness structures. Figure 1 provides a multi-panel
25 view of characteristic growing surface features across the range of our roughness
26 observations. The panels are organized with temperature decreasing toward the bottom and
27 magnification increasing to the right of the figure. The magnification, temperature, pressure,
28 and humidity information from the databars are available for easier viewing in the appendix
29 table A.1.

30 Particularly in panels 1a, 1c, 1d, 1f, and 1g, distinct roughness can be observed on the basal
31 facets of growing crystals as well as the prism facets. The basal plane roughness usually

1 appears less linear and less symmetrically organized than the prismatic strands. Image
2 sequences (typically around 1 frame/s) reveal the dynamic progress of roughening features as
3 they migrate across the ice surface (videos available in supplemental data, see especially
4 BasalRoughnessLayers.mp4 and SingleCrystal.mp4). Figure 1 panels 1g-1i also display
5 evidence of microfaceting on basal and prism facets. Microfaceting could be induced by
6 cycles of growth and sublimation at all temperatures, but was only observed to develop during
7 steady growth at temperatures below -35°C .

8 These data have also confirmed the idea that surface roughness can be enhanced in proximity
9 to a grain boundary between two neighboring crystals (e.g. Pedersen et al. 2011). In panel 1b,
10 it is apparent that the ridges (in the centers of the images) become larger just as the two
11 advancing facets collide, with ridges radiating outward from the impact point. A video of
12 ridge topographic intensification precipitated by colliding ice crystals is available in the
13 supplementary material (ImpactWave.mp4). It is possible that this effect might enhance
14 roughness in aggregates of ice particles or in cloud regions with high collision frequencies,
15 both of which have been found to be particularly common near deep convection, a region that
16 has also been associated with satellite retrievals indicative of severe particle roughening (Cole
17 et al. 2014). Blackford (2007) and Pedersen et al. (2011) also point out that the
18 microstructure of ice along grain boundaries can play an important role in advancing the
19 understanding of the mechanical properties of snowpacks that are susceptible to avalanche, as
20 well as the dynamics of glaciers.

21 **3.1.2 Magnification and contrast effects**

22 Figure 2 shows a four-panel plot of a growing hexagonal ice crystal starting at 762x
23 magnification in panel a. This crystal was grown near -21°C and is being held near
24 equilibrium in this sequence of panels; the crystal was not visibly growing or sublimating
25 across the 57 seconds separating the first and final panel. Mesoscopic topography is not
26 visible in panel a, so the magnification was increased to 2155x (panel b), which made
27 roughness apparent on the prism facets of the ice crystals. However, the basal facet is tilted
28 almost perpendicular to our viewing angle; therefore, we could not see whether any complex
29 surface architecture existed on the basal facet. By increasing the magnification further and
30 adjusting the contrast and brightness of the ESEM, panel c shows that rough surface
31 topography was actually present on the basal facet (at 3625x magnification). A measurement
32 was made of the depth of a prominent terrace in panel d (1.59 microns); this terrace is among

1 the thickest observed during experiments, suggesting that most topographic features have
2 heights well below 1 micron. This pattern was typical of all experiments; only the most
3 prominent surface structures were typically visible at a magnification of 500x-1000x, while
4 closer examination at 1000-5000x would reveal smaller-scale structures and topography on
5 surfaces that had not been resolved at lower magnification, or at sub-optimal aspect,
6 brightness, and contrast.

7 We attempted to extract profiles of surface height from our ESEM micrographs in to calculate
8 the roughness measure $\langle r \rangle$ recently defined by Neshyba et al (2013) in the context of
9 carefully measured mesoscopic striations observed on ice prism facets growing in VPSEM at
10 -45°C :

$$11 \quad r = 1 - \sqrt{\frac{1}{1 + \left(\frac{dy}{dz}\right)^2}}. \quad (1)$$

12 The average roughness $\langle r \rangle$ is determined along the measured profile. In several
13 circumstances, we succeeded in retrieving an approximate profile, but, as indicated by
14 Ulanowski et al. (2014), in most routine SEM imaging circumstances, we found that it was
15 not straightforward to extract this height profile with confidence. Where this profile could be
16 estimating on growing crystals imaged at magnifications similar to those analyzed by
17 Neshyba et al. (~300-500x magnification), we retrieved similar values of roughness near $\langle r \rangle$
18 ≈ 0.05 . Height profiles along several sections of more highly magnified crystals indicated by
19 red rectangles in panels 1f and 1i yielded $\langle r \rangle$ between .10 and .40. Height profiles, and
20 thereby $\langle r \rangle$ values, can be retrieved by careful attention during the imaging process to SEM
21 stage and crystallographic orientation, resolving of crystal edges, or potentially by 3-D
22 reconstruction of equilibrium crystals captured from multiple angles. We found that it was
23 usually not possible to determine height profiles when structures are visible, but near the limit
24 of the image resolution, or where pronounced roughness did not intersect a resolved crystal
25 edge, a common feature in our observations. We also find that the $\langle r \rangle$ metric, much like the
26 subjective perception of roughness, is affected by image magnification and resolution, and in-
27 turn by the minimum sampling interval of the height profile. If, as our observations imply,
28 surface roughness is significant at sub-micron scales that are not well-resolved at 500x
29 magnification, $\langle r \rangle$ values obtained from profiles retrieved at 500x may be underestimating
30 total roughness.

1 **3.1.3 Inhibited growth observations**

2 As expected, with growth experiments occurring on large, rough substrates, we observed that
3 most crystals nucleated at low supersaturation and then grew steadily and at rate in proportion
4 to ice supersaturation values. At temperatures below -30°C , we repeatedly observed crystals
5 where growth became completely stalled, even at moderate supersaturations ($>115\% \text{RH}_i$)
6 that had previously induced growth in that crystal and continued to lead to growth in adjacent
7 crystals. This stalled growth was only observed following a specific cycle of humidity
8 adjustment: the excess vapor supply of a steadily growing crystal was gradually reduced until
9 reaching equilibrium, with observable growth ceasing, and with no sublimation apparent. This
10 equilibrium condition was held for 1-5 minutes, after which the vapor pressure was gradually
11 increased (or temperature decreased) until RH_i exceeded equilibrium by a few percent. In
12 many instances, the original crystal would not resume growth, even though adjacent crystals
13 continued to nucleate and grow. Figure 3 provides time-separated panels illustrating one such
14 event where a crystal previously held at equilibrium failed to grow following a 0.3°C decrease
15 in temperature, despite several nearby crystals nucleating and growing (please see
16 supplemental videos *Inhibited1.mp4*, *Inhibited2.mp4*, and *Inhibited3.mp4* for additional
17 examples). We interpret this an example of side-by-side ice crystals subject to 2 different
18 surface conditions: a) one where steady growth continues at emergent dislocations or
19 stacking faults, likely partly induced by the underlying substrate and b) one where a
20 previously rough surface has been reconditioned by the momentary maintenance of
21 equilibrium vapor pressure, leaving the surface to grow only by 2-D nucleation requiring
22 vapor in excess of a critical supersaturation. The stalled crystal surfaces do not appear to be
23 completely absent of mesoscopic roughness, nor are they observably different than the
24 growing surfaces, implying that the surface condition differentiating separate growth
25 mechanisms is determined at a smaller scale than observable here. The observation of growth
26 at dislocations and 2D nucleations would not be unprecedented -- Sazaki et al. (2010) used
27 interference-contrast microscopy to demonstrate depositional growth in ice via both 2-D layer
28 nucleation and spiral growth steps at screw dislocations. Several recent studies have also
29 suggested that ice up to 243 K does not have a well ordered hexagonal crystal structure.
30 Instead, ice can contain a mixture of cubic and hexagonal sequences which can give rise to
31 roughness on the prismatic faces (Malkin et al., 2012; Kuhs et al. 2012). It has also been
32 shown that the proportion of cubic sequences decreases as ice is heated and the ice tends
33 towards perfect hexagonal ice (Murray and Bertram, 2006; Kuhs et al., 2012). Both of these

1 findings are consistent with the steady growth we observe at low supersaturation as well as
2 the occurrence of inhibited growth when the surface is given the opportunity to anneal
3 emergent stacking faults.

4 **3.2 Sublimating Crystals**

5 In many instances, cycling of vapor pressure was conducted to observe the sensitivity of
6 surface topography to ambient humidity. In the portions of the cycle below equilibrium vapor
7 pressure, a significantly different character to the surface roughness was observed. Instead of
8 regular or spreading ridges, plateaus, and steps, we observed concave, scalloped depressions
9 developing away from the original surface. In the case of poly-crystalline examples (panel
10 4a), the scalloped depressions took on especially dramatic shapes near former grain
11 boundaries, with sharp peaks often evident during advanced sublimation. However, even
12 single-crystal examples did produce marked scalloping (panels 4b-d), which often initiated at
13 the site of roughness produced during previous growth (see supplemental video
14 GrowandSublime.mp4). It appears that the sublimation occurs outward from multiple centers,
15 often at the site of a former ridge or ledge. In fact, on the basal plane, the sublimation can
16 even be seen to produce hexagonal pits (visible in GrowandSublime.mp4 at ~14s) and the
17 scalloping develops partly from the intersection of multiple spreading pits. Furthermore, if the
18 supersaturation was once again increased above equilibrium, the crystal would typically
19 exhibit micro-faceting that initiated along the sharp ridges bounding adjacent sublimation-
20 scallops. The scale of the scalloping can become fairly large (e.g. panel 4a), so it would be
21 surprising that these structures wouldn't be seen by optical microscopy if they were indeed
22 characteristic of sublimation in diffusion-limited regimes—we speculate that this mode of
23 sublimation may be unique to the kinetic attachment regime, and perhaps significant only for
24 very small ice atmospheric ice particles.

25 **3.3 Transported Crystals**

26 As described in section 2.2, ice crystals were grown at low supersaturation, at -50°C , and at
27 ambient lab pressure in an external, freezer-based diffusion chamber and subsequently
28 captured and transported to the ESEM cold stage in a sealed small-volume cell, with
29 conditions maintained at ice/vapor equilibrium until imaging could commence. The goal of
30 this test was to compare the character of surface roughness observed in experiments described
31 in 3.1 and 3.2 with ice crystals grown in conditions more closely approximating cirrus clouds.

1 While not completely isolated like an ice crystal floating in air, the crystals grown in the
2 freezer-chamber grew outward from a fiber, differentiating them from the close substrate
3 contact seen with ESEM-grown crystals. The presence of large partial pressures of Nitrogen
4 and Oxygen provides the other important departure from ESEM-grown crystals. It is
5 important to note that crystals grown within the chamber (Figure 1-5) are firmly within the
6 attachment kinetics growth regime due to the absence of air and therefore low resistance to
7 diffusion. By contrast, the transported crystals were grown at high pressure to fairly large
8 size, representing growth that was within the diffusion-limited regime. The particle-scale
9 habits and aspect ratios are in agreement with measurements by Bailey and Hallett (2004).
10 The habits are qualitatively more elongated than the nearly isometric crystals typically
11 observed in ESEM. The surfaces themselves (Figure 5) clearly exhibit signatures of
12 mesoscopic roughening that are similar to examples of roughness seen in ESEM-grown
13 crystals. However, for most transported crystals, the crystal edges are more intricate than those
14 observed in ESEM and portions of surfaces of some transported crystals do appear smooth
15 even at magnification greater than 1000x, a rare observation in our ESEM-grown crystals.
16 While we took efforts to maintain equilibrium conditions between capture and imaging, we
17 still cannot say with certainty that the crystals were not exposed to some variation in RH;
18 during transport. The transported crystals hint at some significant differences in roughness
19 morphology, but they do provide evidence that crystals grown in air/water mixtures and with
20 minimal support also exhibit mesoscopic roughness with similarity to that observed in ESEM-
21 grown crystals.

22

23 **4. Conclusions**

24 The ESEM images of ice in section 3 confirms the observations on the nature of mesoscopic
25 roughness recently described by several studies (Neshyba et al. 2013, Ulanowski et al., 2014;
26 Pfalgraff et al. 2010, Pedersen et al. 2011, Zimmerman 2007) and also reveals additional
27 patterns of roughness morphology at high magnification, across a wide range of temperatures,
28 on crystal basal facets, sublimating crystals, and crystals grown in air/water vapor mixtures.
29 Light microscopy has generated highly-detailed images of ice crystals (Libbrecht, 2005;
30 Walden et al., 2003), but a combination of working distance constraints, diffraction limits to
31 resolution, and transmitted light illumination have conspired to prevent visible imaging of
32 mesoscopic surface features. We suggest that submicron scale roughness can also be obscured

1 to detection by ESEM imaging, where the probability of resolving mesoscopic surface
2 topography depends on a combination of factors including the size and depth of the features
3 themselves, the magnification and resolution of the micrograph, the brightness and contrast,
4 and the orientation of the ice crystal with respect to the viewing angle. When brightness and
5 contrast are adjusted to optimal levels, increasing the magnification and resolution serves to
6 create a detailed portrait of ice crystal mesoscopic surfaces which in turn can increase the
7 calculated roughness measure $\langle r \rangle$. Furthermore, high magnification images near 10,000x
8 (Figure 6) depict significant roughness on spatial scales below 200 nm, indicating that for
9 modeling of roughness-induced scattering changes, it is not sufficient to consider light
10 scattering only in the geometric optics regime.

11 Because the ice crystals shown here were grown both inside the pure vapor environment of
12 the ESEM and in external air/vapor mixtures, the ubiquitous presence of mesoscopic
13 roughness indicates that the roughening mechanisms are not caused by the ESEM
14 environment alone and are likely to be significant in atmospheric ice. Despite strong
15 similarity in the subjective appearance of roughness morphologies in crystals grown in
16 diffusion-limited vs. attachment kinetics regimes, there do also appear to be significant
17 differences in overall crystal habit, intricacy of crystal edges, as well as some difference in the
18 patterns of mesoscopic roughness. To increase the utility of these observations, these
19 differences should be investigated further and analyzed quantitatively.

20 The current microscopy observations appears to be well-aligned with a growing body of
21 evidence (Baran 2012; Baum et al. 2011; Ulanowski et al. 2006; Yang et al. 2008; Cole et al.
22 2013) suggesting that measured scattering from ice crystals fit a rough surface model more
23 successfully than crystals with presumed smooth-faceted surfaces. Several of the satellite
24 studies also point out that while roughened ice particles are strongly indicated by radiative
25 retrievals, these results have not been able to diagnose the physical morphology or scale of the
26 apparent roughness (Cole et al. 2013; Ulanowski et al. 2014) and that further progress will
27 depend on a combination of in-situ observations and laboratory measurements, such that
28 realistic representations of surface roughness can be integrated into scattering models.

29 We believe that these new observations of prevalent surface topography in ice crystals
30 warrant careful consideration in the scattering models that are used for satellite retrievals of
31 cirrus ice microphysics, and in turn, affect the radiative modeling of cirrus clouds in climate
32 models. Furthermore, the ubiquity of a complex mesoscopic landscape on the surface of ice

1 crystals also has potential wide-ranging impacts to theories of charge transfer in
2 thunderstorms, the heterogeneous chemistry of stratospheric ozone, and the sintering of ice
3 crystals in snowpacks and glaciers. We suggest that the next steps should focus on efforts to
4 examine and quantify roughness in crystals transported from cirrus-analog environments and
5 development of a mixed air/vapor capability for ice crystal growth in ESEM.

6

7

1 **Appendix A.**

2 This appendix is intended to provide additional detail regarding thermodynamic conditions
3 and temperature calibration processes that have been used to infer approximate saturation
4 ratios. Appendix Table A1. also displays the magnification and thermodynamic data
5 measured in the image panels from Figures 1-6.

6 Vapor pressure measurements within the chamber were observed to be repeatable to within
7 approximately 0.4 Pa. Triple-point measurements and ice growth without substrates also
8 showed no discernible systematic error in pressure readings. Reported temperature
9 measurements are made by a thermocouple imbedded in the Peltier cooling sub-stage, several
10 mm below the substrate surface. The surface was consistently observed to be several degrees
11 warmer than the sub-stage thermocouple reading. The magnitude of this difference was not
12 constant – it was observed to vary between +0.6 °C and +6.5 °C. The magnitude of
13 temperature offset appeared to be increased by the following factors: lower overall
14 temperature, increased substrate thickness, lower substrate thermal conductivity, weaker
15 coolant flow through Peltier block, and shorter thermal equilibration time. Despite this
16 variation, in each experiment, once a working temperature was established, the vapor pressure
17 could be gradually increased to induce ice nucleation and growth and then gradually
18 decreased until growth ceased and sublimation was first observed – this balance point was set
19 as the equilibrium vapor pressure and used to calculate the inferred surface temperature based
20 on the Murphy and Koop (2005) formulation for saturated vapor pressure over ice:

$$21 \ln e_i = 9.550426 - 5723.265/T + 3.53068 \ln(T) - 0.00728332 T \quad (A1)$$

22 where e_i is the saturation vapor pressure over ice in [Pa] and T is the ice temperature in [K].

23 Because most experiments involved growth and sublimation induced by vapor pressure
24 adjustments, the variable experimental saturation ratios could be determined relative to the
25 pre-established equilibrium point. In several instances, it was possible to detect slight
26 temperature drift over an hour-long experiment, which could introduce errors of several tenths
27 of a degree in calculated temperatures. Based on these considerations, along with (much
28 smaller) uncertainty in vapor pressure, the calibrated surface temperatures are deemed to be
29 valid +/- 0.3 °C and ice saturation ratio calculations are approximately +/- 4 % confidence.
30 Introduction of additional thermometry points will be undertaken in future work in order to

1 reduce uncertainty in surface temperatures and saturation ratio, enabling quantitative
2 modeling of growth and sublimation rates.

3

4

5

6

7

1 **Acknowledgements**

2 The authors thank J. Poirier at the Princeton Image and Analysis Center for essential technical
3 assistance with ESEM imaging. Research support was generously provided by the Research
4 Corporation Cottrell College Science Award 19914, NASA EPOESS grant #10-0047, and
5 The College of New Jersey

6

7

8

9

10

1 **References**

- 2 Bailey, M. and Hallett, J.: Growth Rates and Habits of Ice Crystals between -20° and -70°C ,
3 *J. Atmos. Sci.* 61, No. 5, 514–554, 2004.
- 4 Baran, A. J. and L. Labonnote, L.: On the reflection and polarization properties of ice clouds,
5 *J. Quant. Spectrosc. Ra.*, 100, 41–54, 2006.
- 6 Baran, A.J.: From the single-scattering properties of ice crystals to climate prediction: A way
7 forward, *Atmos. Res.*, 112, 45-69, 2012.
- 8 Baum, B. A., Yang, P., Heymsfield, A.J., Schmitt, C.G., Xie, Y, Bansemmer, A., Hu, Y.,J.,
9 Zhang, Z: Improvements in Shortwave Scattering and Absorption Models for the Remote
10 Sensing of Ice Clouds, *J. Appl. Meteor. Climatol.*, 50, 1037–1056 , 2011.
- 11 Baum, B.A., Yang, P., Hu, Y., and Feng, Q. The impact of ice particle roughness on the
12 scattering phase matrix, *J. Quant. Spectrosc. Ra.*, 111, 2534-2549, 2010.
- 13 Bennett, H.E. and Porteus, J.O.: Relation Between Surface Roughness and Specular
14 Reflectance at Normal Incidence, *J. Opt. Soc. Am.*, 51, 123-129, 1961.
- 15 Blackford, J.R.: Sintering and microstructure of ice: a review, *J Phys D: Appl Phys*, 40:
16 R355, DOI:10.1088/0022-3727/40/21/R02, 2007.
- 17 Bony, S., Colman, R., Kattsov, V. M., Allan, R. P., Bretherton, C. S., Dufresne, J.-L., Hall,
18 A., Hallegatte, S., Holland, M. M., Ingram, W., Randall, D. A., Soden, B.J., Tselioudis, G.,
19 and Webb, M.: How Well Do We Understand and Evaluate Climate Change Feedback
20 Processes?, *J. Climate*, 19, 3445-3482, 2006.
- 21 Bryant, G.W., Hallett, J., and Mason, B.J.: The epitaxial growth of ice on single-crystalline
22 substrates, *Journal of Physics and Chemistry of Solids*, 12, 189-195, 1960.
- 23 Burkhardt, U. and Kärcher, B.: Global radiative forcing from contrail cirrus, *Nature Climate*
24 *Change*, 1, 54–58, 2011.
- 25 Chepfer, H., Goloub, P., Riedi, J., de Haan, J. F., and Hovenier, J. W.: Ice crystal
26 shapes in cirrus clouds derived from POLDER-1/ADEOS-1, *J. Geophys. Res.*, 106,
27 7955–7966, DOI:10.1029/2000JD900285, 2001.
- 28 Cole, B., P. Yang, B. A. Baum, J. Riedi, L. Labonnote, F. Thieuleux, and S. Platnick:
29 Comparison of PARASOL observations with polarized reflectances simulated
30 using different ice habit mixtures. *J. Appl. Meteor. Clim.*, 52, 186-196, 2013.
- 31 Cole, B., P. Yang, B. A. Baum, J. Riedi, L. Labonnote, 2014: Ice particle habit and
32 surface roughness derived from PARASOL polarization measurements, *Atmos. Chem.*
33 *Phys.*, 14, 3739-3750, doi:10.5194/acp-14-3739-2014, 2014.

1 Connolly, P., Flynn, M., Ulanowski, Z., Chourolatan, T.W., Gallagher, M., and Bower, K.N.:
2 Calibration of the Cloud Particle Imager Probes Using Calibration Beads and Ice Crystal
3 Analogs: The Depth of Field, *J. Atmos. Oceanic Tech*, 24, 1860–1879, 2007.

4 Cotton, R., Osborne, S. Ulanowski, Z., Hirst, E. Kaye, P.H., and Greenaway, R.S.: The
5 Ability of the Small Ice Detector ,SID-2 to Characterize Cloud Particle and Aerosol
6 Morphologies Obtained during Flights of the FAAM BAe-146 Research Aircraft, *J. Atmos.*
7 *Oceanic Technol.*, 27, 290–303, 2010.

8 Dash, J.G., Mason, B.L., and Wettlaufer, J.S.: Theory of charge and mass transfer in ice-ice
9 collisions, *J. Geophys. Res.*, 106, 20395-20402 , 2001.

10 Furukawa, Y., Yamamoto, M., and Kuroda, T. Ellipsometric study of the transition layer on
11 the surface of an ice crystal, *Journal of Crystal Growth*, 82, 665-677, 1987.

12 Garrett, T.J., Gerber, H., Baumgardner, D.G., Twohy, C.H. and Weinstock, E.M.: Small,
13 highly reflective ice crystals in low-latitude cirrus, *Geophys. Res. Lett.*, 30, 2132, DOI:
14 10.1029/2003GL018153, 2003.

15 Gierens, K. M., Monier, M., and Gayet, J.-F.: The deposition coefficient and its role for cirrus
16 clouds, *J. Geophys. Res.*, 108, 4059-4063, 2003.

17 Goodman, J., Toon, O. B., Pueschel, R. F., Snetsinger, K. G., & Verma, S.: Antarctic
18 stratospheric ice crystals, *J. of Geophys. Res. – Atmos.* 94(D14), 16449-16457, 1989.

19 Harrington, J. Y., Lamb, D., and Carver, R.: Parameterization of surface kinetic effects for
20 bulk microphysical models: Influences on simulated cirrus dynamics and structure, *J.*
21 *Geophys. Res.* 114, D06212, DOI: 10.1029/2008JD011050, 2009.

22 Heymsfield, A. J., Schmitt, C., Bansemer, A, Van Zadelhoff, G.J., McGill, M.J., Twohy, C.,
23 and Baumgardner, D.: Effective Radius of Ice Cloud Particle Populations Derived from
24 Aircraft Probes, *J. Atmos. Oceanic Technol.*, 23, 361–380, 2006.

25 IPCC, 2013. *Climate Change 2013 — The Physical Science Basis*. Contribution of Working
26 Group I to the Fifth Assessment Report of the Intergovernmental Panel on Climate Change,
27 Cambridge University Press, Cambridge, 2013

28 Jensen, E.J., Lawson, P., and Baker, B.: On the importance of small ice crystals in tropical
29 anvil cirrus, *Atmos. Chem. Phys.*, 9, 5519-5537, 2009.

1 Kahnert, M., Sandvik, A.D., Biryulina, M., Stamnes, J.J., and Stamnes, K.: Impact of ice
2 particle shape on short-wave radiative forcing: A case study for an arctic ice cloud, *J. Quant.*
3 *Spectrosc. Ra.*, 109, 1196-1218, 2008.

4 Kramer, M. and Coauthors.: Ice Supersaturations and Cirrus Cloud Crystal Numbers, *Atmos.*
5 *Chem. and Phys.*, 9, 3505-3522, 2009.

6 Kuhs, W. F., Sippel, C., Falenty, A., & Hansen, T. C., Extent and relevance of stacking
7 disorder in “ice Ic”. *P Natl. Acad. Sci. USA*, 109(52), 21259-21264, 2012

8 Kuroiwa, D.: Surface topography of etched ice crystals observed by a scanning electron
9 microscope, *J. Glaciol.*, 475-483, 1969.

10 Kuroda, T. and Lacmann, R.: Growth Kinetics of Ice from the Vapour Phase and its Growth
11 Forms, *J. Crystal Growth*, 56, 189-205, 1982.

12 Lamb, D. and Hobbs, P.V.: Growth Rates and Habits of Ice Crystals Grown from the Vapor
13 Phase, *J. Atmos. Sci.*, 28, 1506-1509, 1971.

14 Lamb, D.: Crystal Growth: 2-D or Not 2-D?, *Proc. of 13th Inter. Conf. on Clouds and Precip.*,
15 Reno, NV., 14-18 August 2000, 1221-1224 , 2000.

16 Libbrecht, K.: The physics of snow crystals, *Rep. Prog. Phys.*, 68, 855, DOI:10.1088/0034-
17 4885/68/4/R03, 2005.

18 Magee, N., Moyle, A.M., and Lamb, D.: Experimental determination of the deposition
19 coefficient of small cirrus-like ice crystals near -50°C , *Geophys. Res. Letters*, 33, L17813,
20 DOI: 10.1029/2006GL026665, 2006.

21 Malkin, T. L., Murray, B. J., Brukhno, A. V., Anwar, J., and Salzmann, C. G.: Structure of ice
22 crystallized from supercooled water, *Proceedings of the National Academy of Sciences of the*
23 *United States of America*, 109, 1041-1045, 10.1073/pnas.1113059109, 2012.06.

24 Mauno, P., G. M. McFarquhar, P. Räisänen, M. Kahnert, M. S. Timlin, and T. Nousiainen.:
25 The influence of observed cirrus microphysical properties on shortwave radiation: A case
26 study over Oklahoma, *J. Geophys. Res.*, 116, D22208, DOI: 10.1029/2011JD016058, 2011.

27 McFarquhar, G. M., Um, J., Freer, M., Baumgardner, D., Kok, G. L. and Mace, G.:
28 Importance of small ice crystals to cirrus properties: Observations from the Tropical Warm
29 Pool International Cloud Experiment ,TWP-ICE, *Geophys. Res. Lett.*, 34, L13803, DOI:
30 10.1029/2007GL029865, 2007.

1 McNeill, V. F., Geiger, F. M., Loerting, T., Trout, B. L., Molina, L. T., & Molina, M. J.:
2 Interaction of hydrogen chloride with ice surfaces: The effects of grain size, surface
3 roughness, and surface disorder. *The Journal of Physical Chemistry A*, 111(28), 6274-6284,
4 2007.

5 Mitchell, D. L., Rasch, P., Ivanova, D., McFarquhar, G., and Nousiaine T.: Impact of small
6 ice crystal assumptions on ice sedimentation rates in cirrus clouds and GCM simulation,
7 *Geophys. Res. Lett.*, 35, L09806, DOI: 10.1029/2008GL033552, 2008.

8 Murray, B. J., and Bertram, A. K.: Formation and stability of cubic ice in water droplets,
9 *Phys. Chem. Chem. Phys.*, 8, 186-192, 2006.

10 Nelson, J., and Knight, C.: Snow Crystal Habit Changes Explained by Layer Nucleation, *J.*
11 *Atmos. Sci.*, 55, 1452-1464, 1998.

12 Neshyba, S. P., B. Lowen, M. Benning, A. Lawson, and P. M. Rowe. "Roughness metrics of
13 prismatic facets of ice, *J. Geophys. Res. Atmos.*, 118, 3309–3318, DOI:10.1002/jgrd.50357,
14 2013.

15 Pedersen, C., Mihranyan, A., and Stromme, M.: Surface Transition on Ice Induced by the
16 Formation of a Grain Boundary, *Plos ONE* 6, e24373, DOI: 10.1371/journal.pone.0024373,
17 2011.

18 Peter, T., Marcolli, C., Spichtinger, P., Corti, T., Baker, M.B., and Koop, T.: When Dry Air Is
19 Too Humid, *Science*, 314, 1399-1402, 2006.

20 Pfalzgraff, W.C., Hulscher, R.M., and Neshyba, S.P.: Scanning electron microscopy and
21 molecular dynamics of surfaces of growing and ablating hexagonal ice crystals, *Atmos.*
22 *Chem. Phys.*, 10, 2927-2935, 2010.

23 Saunders, C.P.R. Thunderstorm electrification laboratory experiments and charging
24 mechanisms, *J. Geophys. Res.*, 99, 10773–10779 , 1994.

25 Sazaki, G., Zepeda, S., Nakatsubo, S., Yokoyama, E., & Furukawa, Y: Elementary steps at
26 the surface of ice crystals visualized by advanced optical microscopy. *Proceedings of the*
27 *National Academy of Sciences*, 107(46), 19702-19707, 2010.

28 Schaefer, V. J.: A method for making snowflake replicas. *Science*, 93, pp.239-240, 1941

1 Schnaiter, M., Kaye, P.H., Hirst, E., Ulanowski, Z., and Wagner, R.: Exploring the surface
2 roughness of small ice crystals by measuring high resolution angular scattering patterns.
3 AAPP, 89, Suppl. No. 1, C1V89S1P084, DOI: 10.1478/C1V89S1P084, 2011.

4 Shcherbakov, V., Gayet, J.F., Backer, B., and Lawson, P.: Light Scattering by Single Natural
5 Ice Crystals, American Meteorological Society, 63, 1513-1525, 2006.

6 Sun, W., Hu, Y., Lin, B., Liu, Z., and Videen, G.: The impact of ice cloud particle
7 microphysics on the uncertainty of ice water content retrievals, J. Quant. Spectrosc. Ra.,
8 112, 189-196, 2011.

9 Takahashi, T., and Fukuta, N.: Ice crystal replication with common plastic solutions. J.
10 Atmos. Ocean. Tech., 5(1), 129-135, 1988.

11 Truby, F. K.: Hexagonal microstructure of ice crystals grown from the melt. J. Appl. Phys.,
12 26(12), 1416-1420, 1955.

13 Ulanowski, Z., Hesse, H., Kaye, P.H., Baran, A.J.: Light scattering by complex ice-analogue
14 crystals, J. Quant. Spectrosc. Ra., 100, 100(1), 382-392, DOI: 10.1016/j.jqsrt.2005.11.052,
15 2006.

16 Ulanowski, Z., Hirst, E., Kaye, P.H., and Greenaway, R.: Retrieving the size of particles with
17 rough and complex surfaces from two-dimensional scattering patterns, J. Quant. Spectrosc.
18 Ra., 113(18), 2457-2464, DOI: 10.1016/j.jqsrt.2012.06.019, 2012.

19 Ulanowski, Z., Kaye, P.H., Hirst, E., and Greenaway, R.S.: Light scattering by ice particles in
20 the Earth's atmosphere and related laboratory measurements, Procs. 12th Int. Conf. on
21 Electromagnetic and Light Scattering: ELS'XII, June 28-July 2, 2010, Helsinki, Finland, 294-
22 297, 2010.

23 Ulanowski, Z., Kaye, P. H., Hirst, E., Greenaway, R. S., Cotton, R. J., Hesse, E., & Collier, C.
24 T. (2014). Incidence of rough and irregular atmospheric ice particles from Small Ice Detector
25 3 measurements. Atmos. Chem. Phys., 14(3), 1649-1662, 2014.

26 Um, J. and McFarquhar, G.M.: Dependence of the single-scattering properties of small ice
27 crystals on idealized shape models, Atmos. Chem. Phys., 11, 3159-3171, 2011.

28 Walden, V.P., Warren, S.G., and Tuttle, E.: Atmospheric Ice Crystals over the Antarctic
29 Plateau in Winter, American Meteorological Society, 42, 1391-1405, 2003.

1 Wergin, W.P., Rango, A., and Erbe, E.F.: Observations of Snow Crystals Using Low-
2 Temperature Scanning Electron Microscopy, *Scanning*, 17, 41-49, 1995.

3 Yang, H., Dobbie, S., Herbert, R., Connolly, P., Gallagher, M., Ghosh, S., Al-Jumur, S. M. R.
4 K. and Clayton, J.: The effect of observed vertical structure, habits, and size distributions on
5 the solar radiative properties and cloud evolution of cirrus clouds, *Q. J. Roy. Meteor. Soc.*,
6 138(666), 1221-1232, 2012.

7 Yang, P. and Liou, K.N.: Single-Scattering Properties of Complex Ice Crystals in Terrestrial
8 Atmosphere, *Contr. Atmos. Phys.*, 71, 223–248 , 1998.

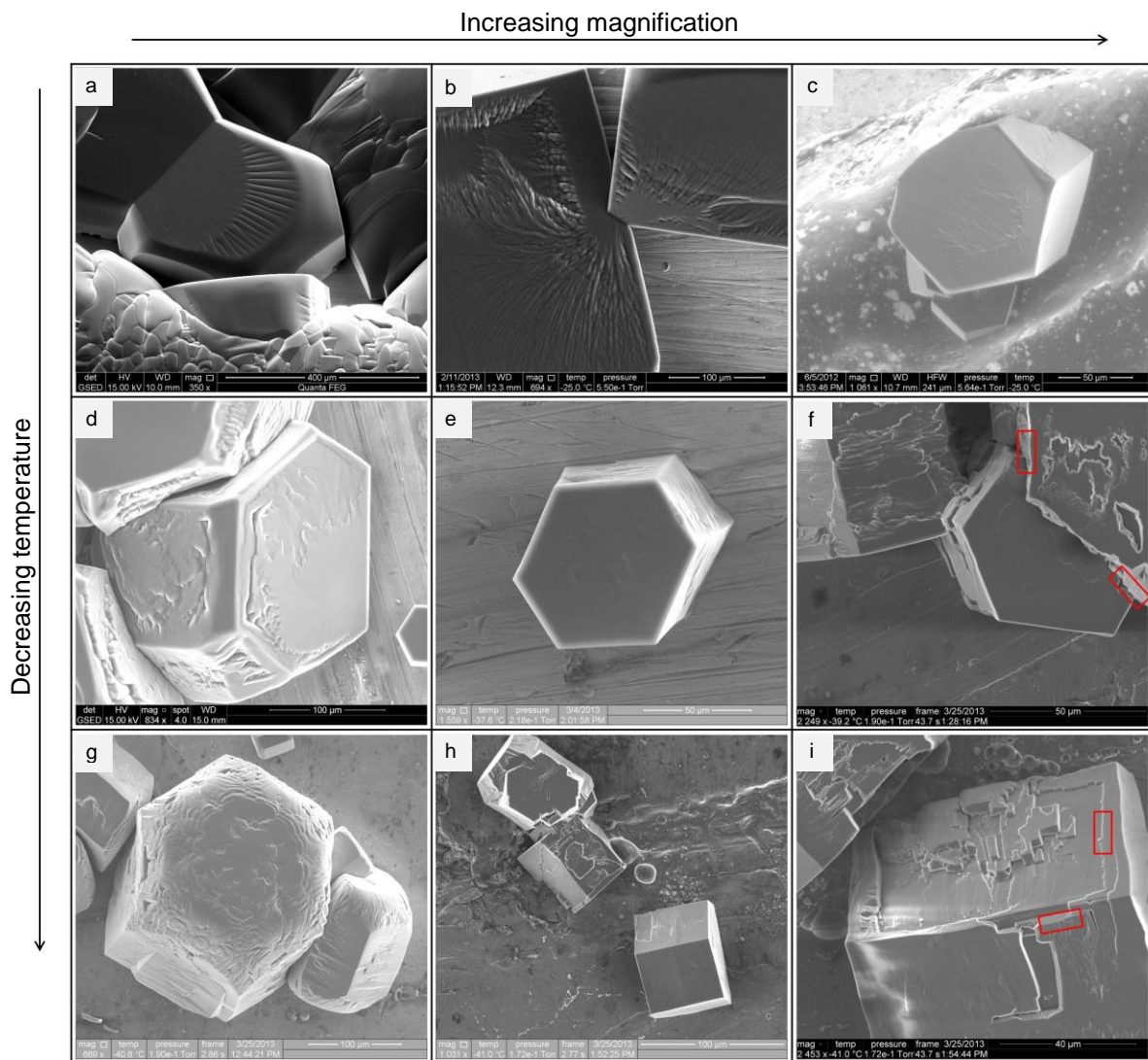
9 Yang, P., Hong, G., Kattawar, G., Minnis, P., and Hu, Y.: Uncertainties Associated With the
10 Surface Texture of Ice Particles in Satellite-Based Retrieval of Cirrus Clouds: Part II--Effect
11 of Particle Surface Roughness on Retrieved Cloud Optical Thickness and Effective Particle
12 Size, *IEEE Transactions on Geoscience and Remote Sensing*, 46, 1948-1957, 2008.

13 Yang, P., Bi, L., Baum, B. A., Liou, K. N., Kattawar, G. W., Mishchenko, M. I., & Cole, B.,
14 Spectrally Consistent Scattering, Absorption, and Polarization Properties of Atmospheric Ice
15 Crystals at Wavelengths from 0.2 to 100 μ m., *J. Atmos. Sci.*, 70(1), 330-347, 2013.

16 Yi, B., Yang, P., Baum, B. A., L'Ecuyer, T., Oreopoulos, L., Mlawer, E. J., Heymsfield, A.J.
17 and Liou, K. N, Influence of ice particle surface roughening on the global cloud radiative
18 effect, *J. Atmos. Sci.*, *J. Atmos. Sci.*, 70, 2794–2807, DOI: 10.1175/JAS-D-13-020.1, 2013.

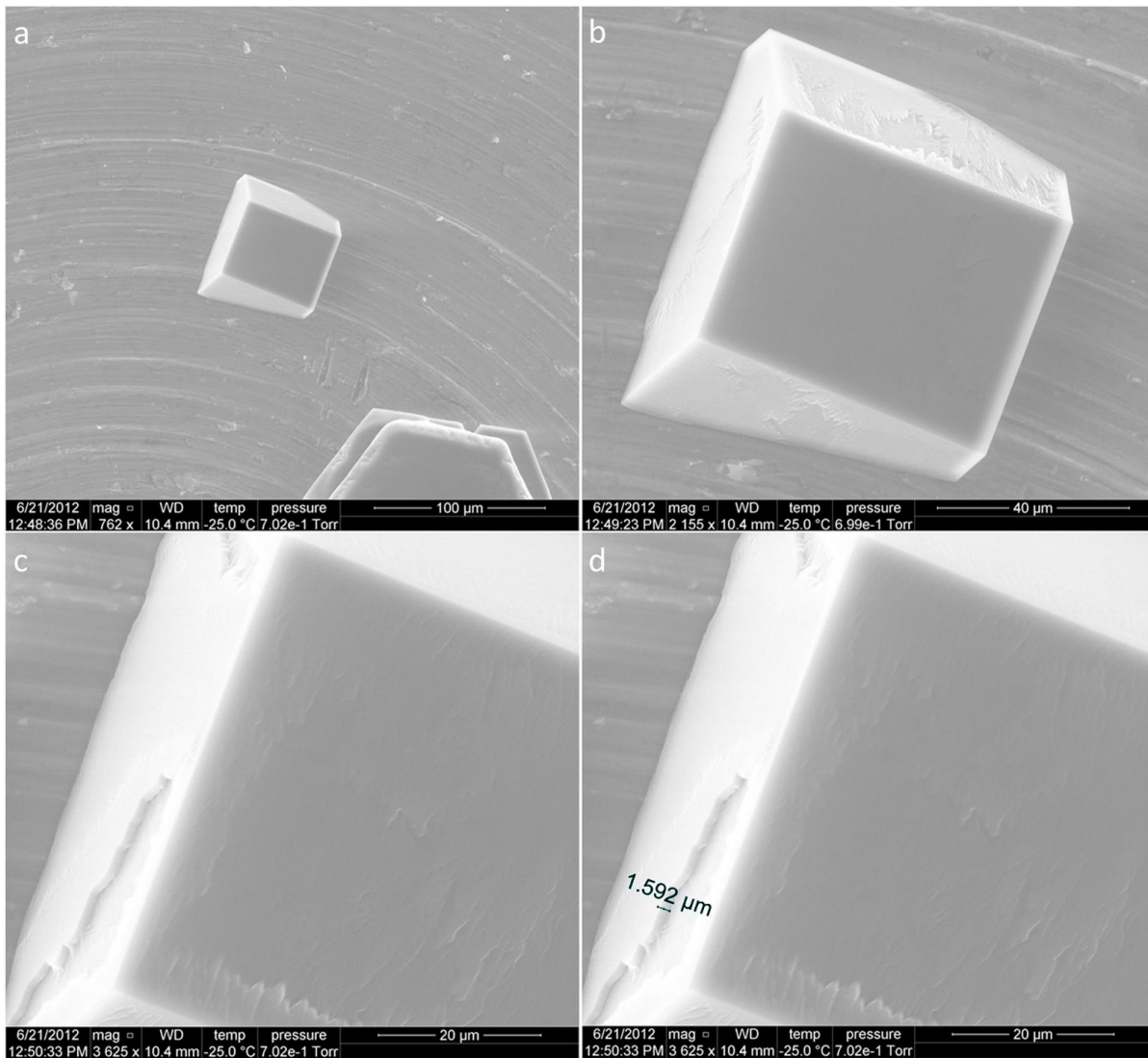
19 Zimmermann, F., Ebert, M., Worrigen, A., Schutz, L., and Weinbruch, S.: Environmental
20 scanning electron microscopy, ESEM as a new technique to determine ice nucleation
21 capability of individual atmospheric particles, *Atmospheric Environment*, 41, 8219-8227,
22 2007.

23
24
25
26
27
28
29
30
31



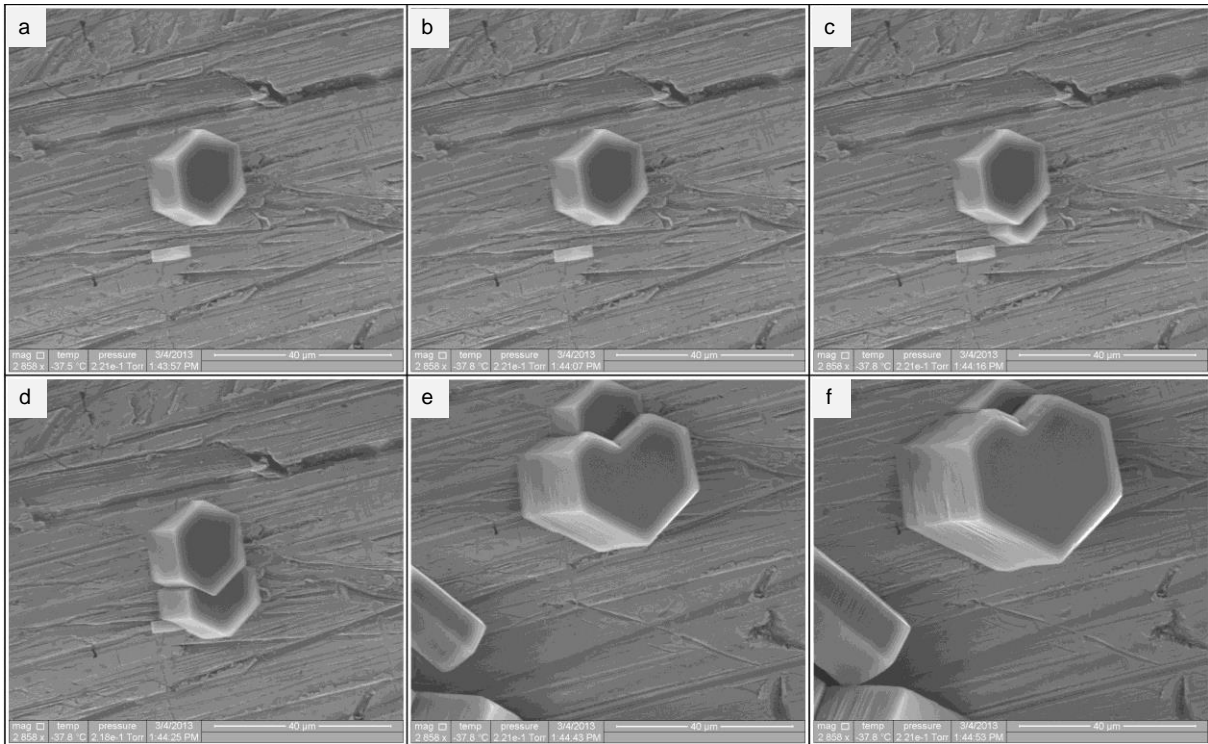
1
 2 Figure 1: Image panels at a variety of magnification, temperatures, and pressures -- all
 3 showing various examples of mesoscopic surface topography. Red rectangles in panels 1f
 4 and 1i show sites used for calculating roughness measure $\langle r \rangle$. Data detail available in
 5 appendix table A.1.

6



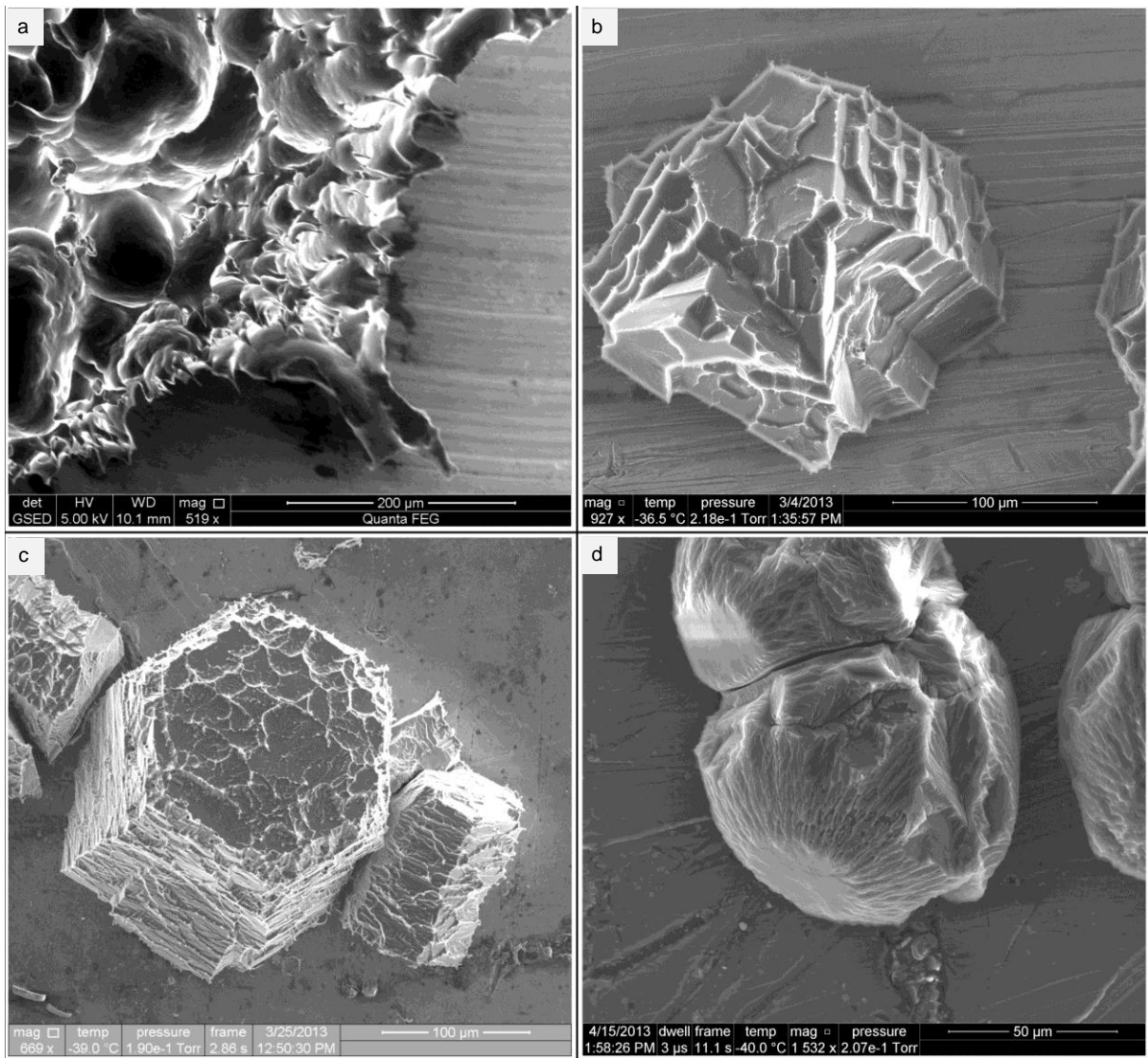
1
2
3
4
5
6

Figure 2. Demonstration of increased magnification effect upon perceived roughness is shown here, as well as a measurement of ridge depth (panel d). Data detail available in appendix table A.1.



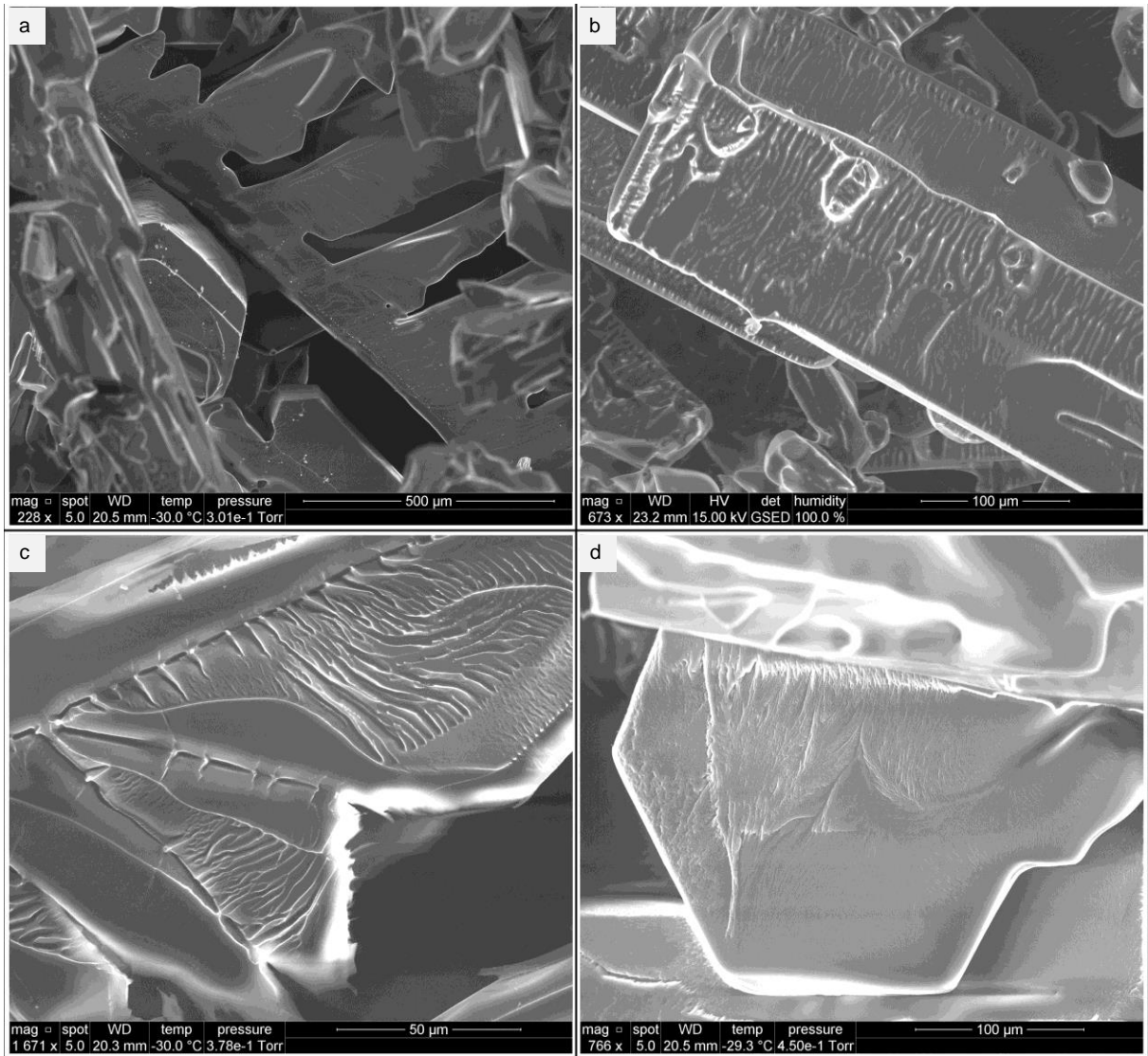
1
 2 Figure 3: Series of frames separated by ~10s (20 s between panel d and e as the acquisition
 3 was re-centered to capture growing crystals at bottom-left in panel d and e). The original 2
 4 crystals at equilibrium in panel a. do not grow when subjected to a temperature decrease of
 5 0.3°C (equivalent to ~105 RH_i), with vapor pressure held constant. Data detail available in
 6 appendix table A.1.

7



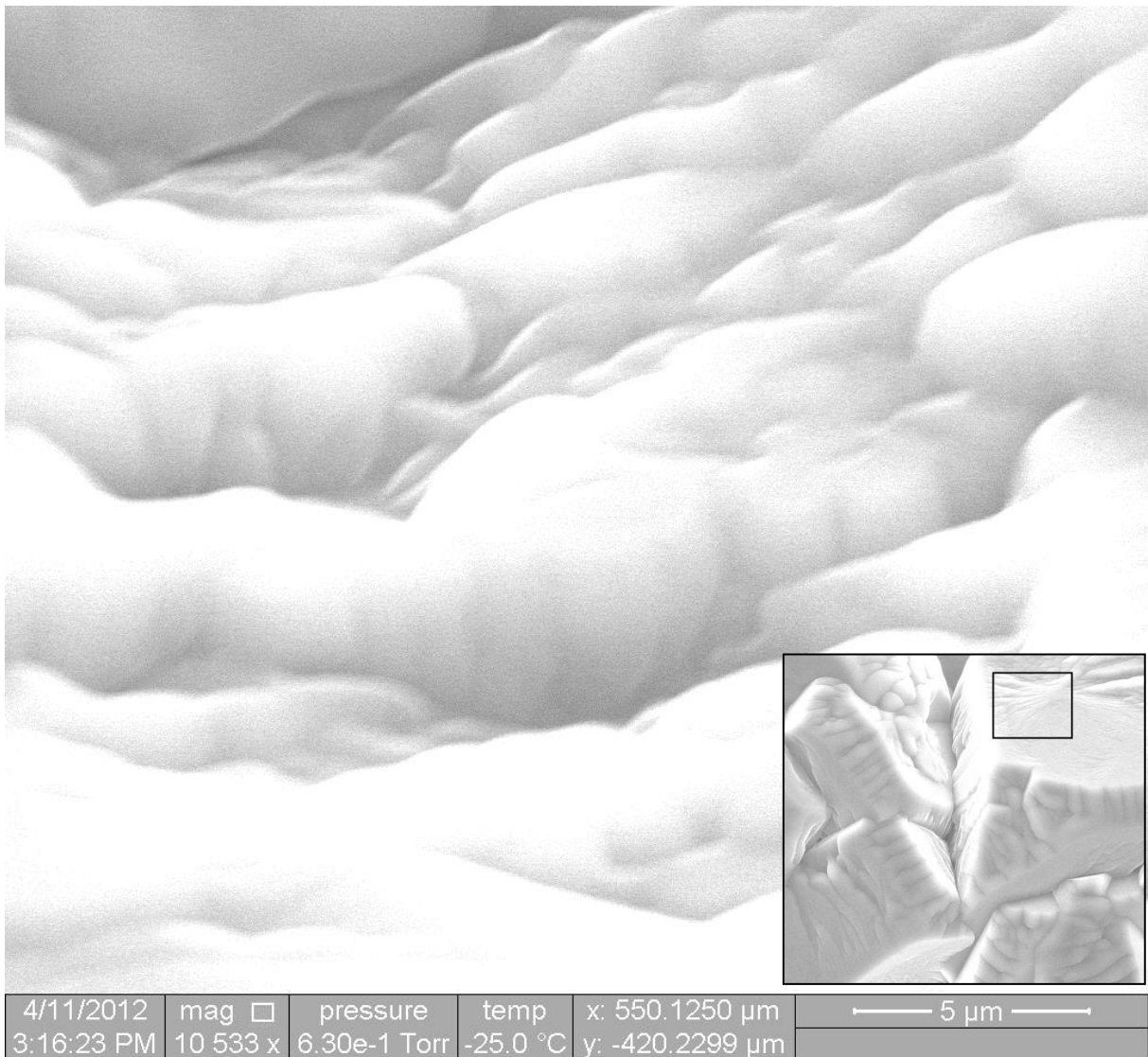
1
 2 Figure 4: Sublimating ice crystals displaying scalloped depressions and sharp ridges and
 3 peaks of roughness. Panel a. was originally composed of a polycrystalline ice particle, with
 4 peaks and ridges prominent at former grain boundaries. Data detail available in appendix table
 5 A.1.

6
 7



1
2
3
4
5
6
7

Figure 5: Transported ice crystals, showing portions of 4 different crystals grown at $-50\text{ }^{\circ}\text{C}$ in a static diffusion chamber between 100 and 105% RH_i . The crystals were maintained in cryogenic equilibrium during transport into the ESEM for imaging under vapor-matched saturation conditions. Data detail available in appendix table A.1.



1
2
3
4
5
6
7

Figure 6: Ice crystals are observed at high magnification, the highest we were able to attain without sacrificing the quality of the image. Inset image (1903x magnification) shows the location of the high-magnification zoom, located on the basal facet of a growing crystal, and near to the intersection of the adjoining prism facet with another crystal’s basil facet. Data detail available in appendix table A.1.

1

Panel	Magnification	Vapor Pressure (Pa) {+/- 0.5 Pa}	Sub-stage Temp. (°C) {+/- 0.1 °C }	Calibrated surface Temp. (°C) {+/- 0.3 °C }	Ice Saturation Ratio {+/- 4%}
Figure 1					
a	350	73.3	-25.0	-24.0	1.05
b	694	73.3	-25.0	-24.0	1.05
c	1061	75.2	-25.0	-23.9	1.06
d	834	n/a	n/a	n/a	n/a
e	1559	29.1	-37.6	-33.8	1.14
f	2249	25.3	-39.2	-35.2	1.13
g	669	25.3	-40.6	-35.5	1.20
h	1031	22.9	-41.0	-36.0	1.14
i	2453	22.9	-41.0	-36.0	1.14
Figure 2					
a	762	93.6	-25.0	-22.0	1.00
b	2155	93.2	-25.0	-22.0	1.00
c	3625	93.6	-25.0	-22.0	0.99
d	3625	93.6	-25.0	-22.0	1.00
Figure 3					
a	2858	29.5	-37.5	-32.6	1.02
b	2858	29.5	-37.8	-32.9	1.05
c	2858	29.5	-37.8	-32.9	1.05
d	2858	29.1	-37.8	-32.9	1.04
e	2858	29.5	-37.8	-32.9	1.05
f	2858	29.5	-37.8	-32.9	1.05
Figure 4					
a	519	n/a	n/a	n/a	n/a
b	927	29.1	-36.5	-32.0	0.94
c	669	25.3	-39.0	-33.5	0.96
d	1532	27.6	-40.0	-33.0	0.99
Figure 5					
a	228	40.1	-30.0	-29.4	1.00
b	673	n/a	n/a	n/a	n/a
c	1671	50.4	-30.0	-27.3	1.00
d	766	60.0	-29.3	-25.5	1.00
Figure 6					
a	10533	84.0	-25.0	-22.4	1.05

2

3 **Table A.1** Magnification, temperature, vapor pressure, and calculated saturation ratios for
4 images figures.

5